Picosecond laser texturing of Al current collector to improve cycling performances and simplify recycling of Lithium-ion batteries

Surfaces and Interfaces 51 (2024) 104659

Contents lists available at ScienceDirect

Surfaces and Interfaces

journal homepage: www.sciencedirect.com/journal/surfaces-and-interfaces

Picosecond laser texturing of Al current collector to improve cycling performances and simplify recycling of Lithium-ion batteries

Paolo Tallone [a,*], Silvia Spriano [a], Daniele Versaci [a], Sara Ferraris [a], Alice Tori [b], Silvia Bodoardo [a]

[a] Politecnico di Torino, Department of Applied Science and Technology, Corso Duca degli Abruzzi, 24, 10129 Turin, Italy
[b] Osai Automation Systems SpA, Via della Cartiera 4, 10010 Parella TO, Italy

ARTICLE INFO

Keywords:
Laser texturing
Current collector
Cathodes
Recycling
Li-ion battery

ABSTRACT

Lithium-ion batteries (LIBs) are one of the main energy storage technologies currently in use and recycling them offers significant economic, environmental, and material recovery benefits. Despite various recycling processes, separating the metallic current collector from the electrode composite film remains a crucial challenge. In this framework, the present study focuses on laser texturing of aluminum current collectors (CCs) to introduce a microscale surface architecture. The asymmetric surface pattern facilitated a controlled and directional adhesion, enhancing attachment to manage the significant volume variation of the active material (NMC811) during charging and discharging cycles. Additionally, it enabled an easy separation of the electrode composite layer from the current collector, during recycling, by applying a force in a specific direction. As a result, the laser-treated cathodes displayed low electrode polarization and increased cycling performances, with a capacity retention of 67.6% after 300 cycles at 1C, thanks to the increased interfacial adhesion that reduced the active material delamination from the current collector upon cycling.

1. Introduction

Lithium-ion batteries are extensively used in portable electronics such as mobile phones, laptops and many other common devices due to their high energy density, high power density and long lifespan [1]. Nowadays, a growing demand for LIBs is generated by the automotive industry due to the fundamental role of battery technology in the decarbonization [2] and electrification of the transportation sector [3]. Researchers and analysts forecast that the rapid penetration of LIBs in electric mobility will lead to an estimated demand of >500 GWh energy production in 2025 and >2000 GWh by 2030 [4]. Within this context, the quantity of spent LIBs will present a similar tendency [5], and how to dispose of this large amount will constitute a crucial challenge [6]. At the same time, the development of cell designs that can achieve high electrochemical performances during the battery lifetime and can render the recovery of valuable materials during battery recycling is therefore crucial [7]. A common critical issue during the recycling process is the separation of the active material coating from the current collector [8,9].

At present, copper (Cu) and aluminum (Al) current collectors are generally used at the anode and the cathode side of the battery, respectively [10,11]. The main role of the current collector is structural as well as electrochemical, as fast and easy migration of electrons to and from the active material particles must be ensured to allow the electrode to withstand high current densities. Good adhesion between the current collector and the composite active material film is therefore crucial in to guarantee good electrochemical performances of the electrode. Moreover, delamination of the active material particles is regarded as one of the common causes of capacity fading of the battery, making the contact between CC and active material an even more fundamental parameter. On the other hand, at the end of the battery life, easy delamination of the composite film from the metallic foil is required to recover critical raw materials [12].

Current trends on the surface modification of the current collectors are mainly focused on increasing the adhesion between the CCs and the active material coating as well as on increasing the corrosion resistance of the metal. Various methods have been proposed, including etching [13] the CC surface with strong acids or bases to increase the surface roughness and therefore improve the electrochemical performances of the electrodes . Another common approach is to coat the current

* Corresponding author.
E-mail address: paolo.tallone@polito.it (P. Tallone).

https://doi.org/10.1016/j.surfin.2024.104659
Received 8 May 2024; Received in revised form 11 June 2024; Accepted 20 June 2024
Available online 20 June 2024

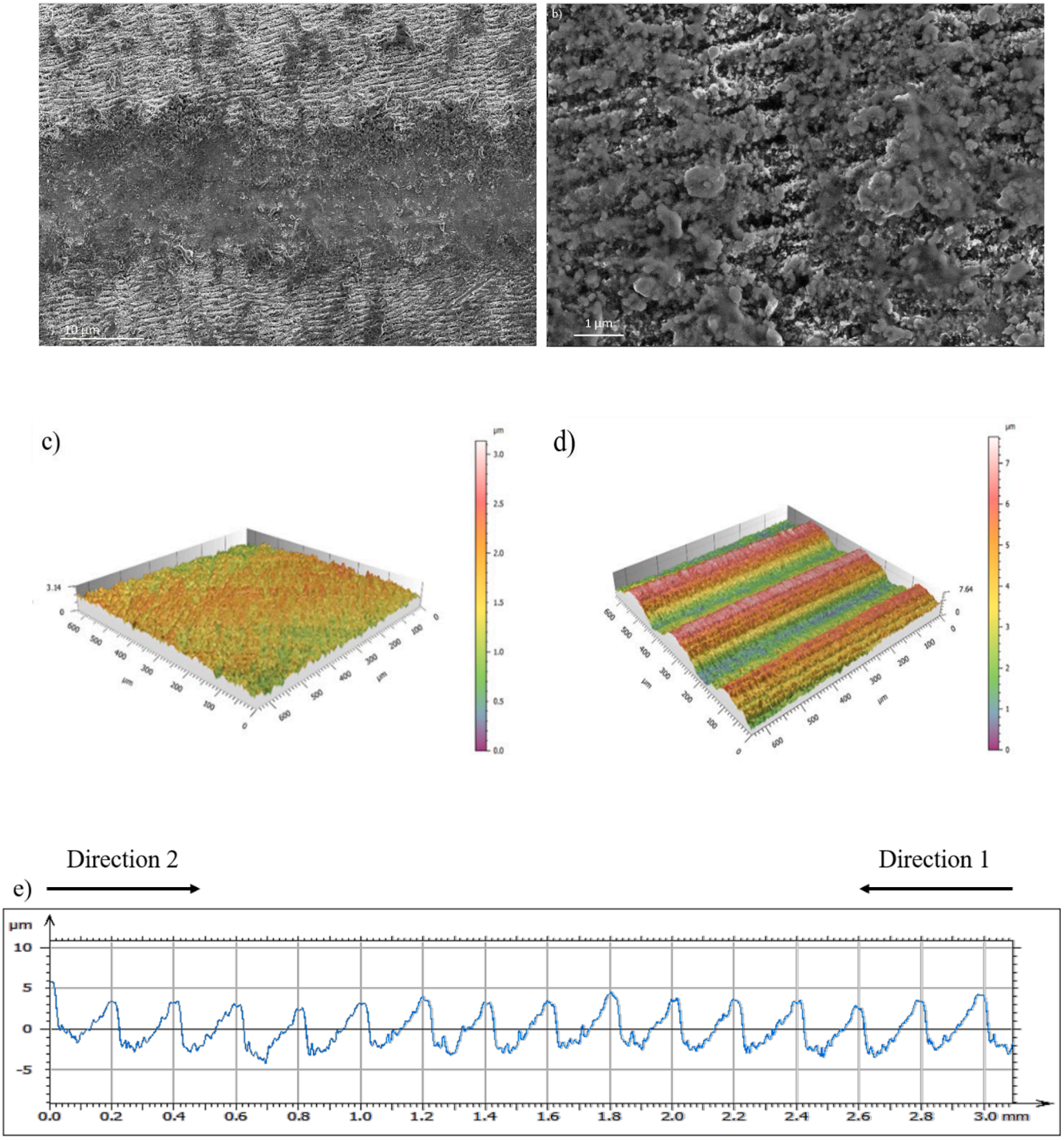

Fig. 1. SEM micrographs of the Laser Textured Al CC at magnifications of a) 5kX and b) 30 kX. Optical profilometry 3D images of the surface of the c) pristine Al CC and d) Laser Textured Al CC. e) Contact profilometry line scan of the asymmetric grooves obtained on the Laser Textured Al CC. The direction 1 and 2 (arrows) are related to the adhesion measurements described in Section 3.2.

collector [14], also improving the corrosion resistance properties of the metal [15]. These different chemical techniques are effective [16,17] but require the use of expensive and toxic chemicals, thus reducing the overall sustainability of the production process. The use of more environmentally friendly methods is therefore crucial in the development of more efficient current collectors.

The use of laser technology in battery production has gained attention over the years regarding the cutting of the electrodes and separators [18,19] as well as for the welding of the cell tabs [20]. More recently, this technology has been introduced also within the electrode manufacturing process [21]. Some studies have been published on the laser ablation of part of the active material coating to improve the wettability [22,23] of the electrode during the liquid electrolyte injection, therefore reducing production costs [24].

Pulsed laser ablation has been regarded as a promising technique for the Laser Surface Texturing (LST) of thin metallic foils to increase the active surface area without causing excessive mechanical damage. By optimizing the process parameters, precise control of the three-dimensional structure of the surface is achievable.

Various studies have been published on this topic, with the main goal

of using LST techniques to improve the mechanical adhesion of the active material layer to the current collector surface [25] to enhance the electrochemical performances of the electrode, achieving promising results both for the cathodic [26,27] and the anodic sides [28,29]. On the other hand, the environmental and economic issues related to the battery End of Life were not faced.

To the authors' knowledge, a single study has focused on the creation of a suitable asymmetric geometry on the CC surface to achieve directional adhesive properties, but using mechanical methods and without assessing the electrochemical performances of the textured electrodes [30].

In this work, we propose a picosecond laser-based surface texturing method able on one hand to generate triangular asymmetric features on the current collector surface in a fast and efficient way.

2. Material and methods

2.1. Laser texturing of the aluminum current collector

Laser texturing was performed using a Nd:YAG 1064 nm laser (HyperRapid NX model, Coherent, Germany) with a pulse duration < 15 ps. Beam movement and focusing were achieved with a galvanometric scanning head equipped with a 160 mm focal length f-theta lens. A parallel line scanning strategy and different scanning speeds was utilized to achieve the desired surface geometry at a selected power of 25% of the maximum power at a repetition rate of 200 kHz. All the experiments were performed in air.

2.2. Morphology characterization of laser textured current collectors

The surface morphology was observed by means of Scanning Electron Microscopy (SUPRA ZEISS FE-SEM) coupled with Energy-dispersive X-ray spectroscopy (EDS). Sectioned electrodes were also prepared and mounted in resin while being held vertically with a clip. The samples were then lapped to expose the cross-section of the electrodes. The surface topography was measured through Confocal Microscopy (LSM 900, ZEISS, Oberkochen, Germany) and Contact Profilometry (Taylor Hobson Intra Touch 3D. The surface roughness parameters were obtained following the ISO 25,178 standard procedure.

2.3. Cathode preparation and electrochemical characterization

Working electrodes were prepared by the solvent tape casting method. An N-Methyl-2-pyrrolidone (NMP, Sigma-Aldrich) based cathodic slurry was prepared by mixing Lithium Nickel Manganese Cobalt Oxide (NMC811, MTI Corporation), Carbon Black C—NERGY C65 (Imerys Graphite & Carbon Corporation) and polyvinylidene difluoride (PVDF, Arkema) at a weight ratio of 90:5:5 wt.%, respectively. For preparation of the slurry, PVDF was dissolved in NMP to obtain 8 wt.% solutions. After complete binder dissolution, the solid fraction (active material + carbon black) was added to the solution and the slurries were mixed using a ball mill for 20 min at 15 Hz. Subsequently, the obtained slurries were cast onto pristine and laser-textured aluminum current collectors (battery grade, MTI Corporation) by the Doctor Blade technique using an automatic film applicator (Sheen 1133 N, speed of 10 mm s^{-1}) to obtain pristine (P-NMC) and laser textured (L-NMC) electrodes. After solvent evaporation in air at 50 °C for 1 h, 1.766 cm^2 disks were punched out with a Compact Precision Disc Cutter MSK-T-07 and vacuum dried at 120 °C (Büchi Glass Oven B-585) for 4 h, before cell assembly. The active material mass loadings explored in this work were in the range of 8–8.6 mg cm^{-2}. Cell assembly was carried out in an Ar-filled glove box (MBraun Labstar, H_2O and O_2 content <1 ppm) using a two-electrode 2032 coin cell configuration. Glass fibre (Whatman GF/D) was used as a separator and soaked with an electrolyte solution of $LiPF_6$ 1 M 1:1 v/v mixed with ethylene carbonate (EC) and diethyl carbonate (DEC) (Solvionic). NMC811 cathodes were electrochemically tested at RT using Li disk counter electrodes (Ø 16 mm, thickness 0.6 mm, Tobmachine). The cycling performance of cells was assessed through galvanostatic discharge–charge cycling (GC) on an Arbin LBT-21,084 at different current regimes in the voltage range 2.8 – 4.3 V. Electrochemical impedance spectroscopy (EIS) characterisation and Cyclic Voltammetry (CV) were conducted on a versatile multichannel potentiostat (VMP-3 Biologic). Impedance measurements were performed after different cycles of charge–discharge at 0.1C with a 10 mV amplitude in the 100 kHz – 1 MHz frequency range. CV measurements were performed with a scanning speed of 0.1 mV s^{-1}. Intermitted Current Interruption (ICI) measurements were employed to assess the Internal Resistance of the cells with P-NMC and l-NMC electrodes at different lithiation states by an Arbin LBT-21,084. Specifically, the ICI test was performed by charging/discharging the battery at a galvanostatic current of 0.1C for an interval of 5 min, relaxing for 5 s and repeating this process again until the cut-off voltage was reached.

Table 1
Results of EDS analyses performed on pristine and laser-textured aluminum current collectors.

Element	P-Al%	L-Al%
Aluminum	98.71	97.26
Oxygen	1.29	2.74

2.4. Adhesion tests

Scratch tests were performed using an MCT3 tester (Antoon Paar) equipped with a wedge blade indenter in the load range 0.03–3 N with a loading rate of 1–3 $Nmin^{-1}$. Five scratches were performed for each sample, with a spacing of 3 mm. l-NMC electrodes were subjected to scratches in opposite directions, perpendicularly to the scanning lines of the laser texturing process to evaluate the directional adhesion properties of the textured CC.

3. Results and discussion

3.1. Laser textured CCs morphological characterization

The surface morphology of the laser-textured (L-Al) and pristine (P-Al) current collector was observed by means of SEM. As can be observed in Fig. 1, the textured electrode displays micro and nanostructured features induced by the laser treatment. An untreated area is observable in Fig. 1a to appreciate the difference. Notably, Laser Induced Periodic Surface Structures (LIPSS) are visible on the surface. At higher magnification, micrometric features and particles are observed, related to limited surface oxidation induced by the laser texturing performed in the air. This was also confirmed by EDS analysis (Table 1), which showed a slight increase in the oxygen amount when compared to the pristine aluminum CC. This surface oxidation was not detrimental to the electrochemical performances of the textured electrodes, as shown below. It is worth mentioning that a small and controlled quantity of Al_2O_3 can potentially be beneficial for the corrosion resistance properties of the aluminum surface, considering the increased surface area due to the texturing and especially in the presence of electrolytes with fluorinated salts such as $LiPF_6$. A small increase in the Al_2O_3 quantity on the CC surface can therefore limit the electrode degradation and extend the LIB cycle life [31,32].

Confocal Microscopy was used to obtain three-dimensional views of the sample surface and Contact Profilometry was used to scan the sample perpendicularly to the generated asymmetric grooves in order to obtain a line profile. As can be observed in Figs. 1c-e, asymmetric triangular structures were obtained through laser texturing. These micrometric structures were intentionally generated to achieve the directional adhesion of the active material coating on the textured Al CC. The roughness parameters were also obtained both for the pristine and

Table 2
Values of the Surface Roughness parameters obtained through optical confocal microscopy according to the ISO 25,178 standard procedure.

Parameter	P-Al μm	L-Al μm
Sq	0.192	1.70
Ssk	−0.172	−0.132
Sku	3.11	1.73
Sp	0.661	3.54
Sv	1.05	3.61
Sz	1.71	7.15
Sa	0.153	1.50

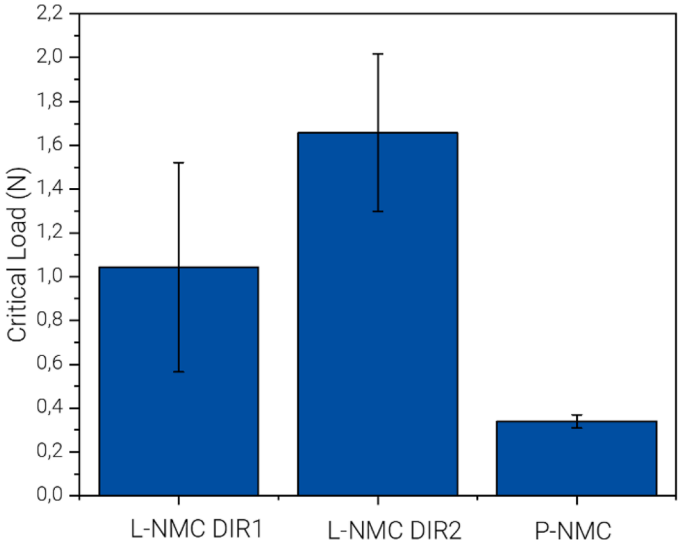

Fig. 2. Micro-scratch analysis results of the critical loads measured on the P-NMC and the l-NMC samples.

the textured electrodes. The results are summarized in Table 2. The Sa parameter, representing the difference in height of each point compared to the mean plane of the surface within the defined area, is the most commonly used parameter to evaluate the surface roughness. As expected, its value was increased by the LST of the surface. Sp is the maximum peak height and Sv is the maximum valley depth. The maximum height of surface Sz is the sum of the maximum peak height Sp and maximum valley depth Sv. All these parameters are characteristics of the surface amplitude and were all increased by laser texturing of the CC surface. The Skewness (Ssk) and Kurtosis (Sku) characterize the height distribution of the surface. Negative values of Ssk indicate a height distribution skewed above the mean plane and vice versa. Ssk values were negative both for P-Al and l-Al, but the textured surface showed a slight shift towards less negative values. The Sku represents the sharpness of the surface profile: values higher than 3 indicate the presence of pointed and sharp peaks, as for the P-Al surface, whereas smaller values are related to shapes rounder than a Gaussian distribution, as the one generated by laser texturing. The surface area increase was evaluated elaborating the 3D reconstructions through the Gwyddion software. The scanned sample area was 639 × 639 μm, giving rise to a projected area of 0.4082 mm^2 for both the P-Al and the l-Al. The measured surface area was 0.4101 mm^2 for the P-Al and 0.4410 mm^2 for the l-Al. Compared to the projected area, the increase was low for the P-Al (0.46%) and much higher (8.04%) for the l-Al sample, proving the increased surface area generated by the Laser Surface Treatment.

3.2. Adhesion measurements

Adhesion of the active material coating to the current collector was evaluated for the P-NMC and the l-NMC electrodes by means of micro-scratch analysis. This technique allows the critical load measurement in different directions and was employed to evaluate adhesion differences in opposite directions, perpendicularly to the triangular asymmetric surface features for the l-NMC electrode. The P-NMC sample was examined as a reference. The results are reported in Fig. 2, where the increased adhesion between the textured electrode and the untextured one is evident, due to the higher surface area of the l-NMC current collector, as evidenced also in the previous section. More importantly, the critical load for the l-NMC electrode along direction 1 (average of 1.04 N, standard deviation of 0.48) was statistically lower than the one measured along direction 2 (average of 1.66 N, standard deviation of 0.36). An analysis of variance (ANOVA) was conducted to evaluate the statistical difference between the two means. The obtained F value is 5.34, the obtained p value is 0.0496, indicating a significant effect ($p < 0.05$) of the scratch direction on the measured critical load. In other words, the increased adhesion was present regardless of the delamination direction, but it was less pronounced along direction 1. As previously reported by Jin et al. [30], an asymmetric surface geometry similar to the one described in this work is able to generate a directional adhesion between the current collector and the active material coating. This phenomenon is related to the different paths followed by the crack along the two directions during the delamination process. This peculiar property can potentially make a significant contribution to the production of easy to recycle high-performance lithium-ion batteries, considering also the improved electrochemical performances of the l-NMC electrodes highlighted in the next sections of this work.

3.3. Electrochemical characterization

The cathodes, after preparation, underwent different electrochemical assessments in a half-cell setup, employing a lithium metal disk as a counter electrode. The cycling performance of the cells prepared was initially evaluated concerning their rate capability. The cells underwent galvanostatic charge and discharge cycles at different C-rates of 0.1C, 0.2C, 0.5C, 1C, 2C, 3C, 4C, and 5C.

The performance comparison between electrodes with textured and untextured CC highlighted similar results at every C-rate (Fig. 3a). The error bars are related to three repetitions of the experiment for each type of cell, to ensure reliability and replicability of the experimental data. Thus, the laser surface texturing of the current collector did not seem to affect the rate capability of the cell. This effect is evident in Fig. 3b-c, where charge-discharge curves at different C-rates are reported for each type of CC. As can be observed, the charge/discharge profiles were similar at every C-rate for the two samples. After the activation cycles at 0.1C, a slight increase in the discharge capacity was observed at 0.2C for the l-NMC electrode, but not for the P-NMC. This variability in the first cycles could be related to the permeation of the electrolyte within the porosity of the electrode during the first formation cycles. This effect was probably associated with the high mass loading of the electrodes. The specific capacity remains comparable at every C-rate. For instance, at 2C both samples exhibited a specific capacity of about 128 mAh g^{-1}, whereas at 5C the specific capacity was 45 mAh g^{-1} for the two electrodes. Notably, an increased separation (polarization) between the charging and discharging curves was evident at higher C-rates (Fig. 3d). Interestingly, this separation was lower for the l-NMC electrode. From the rate capability tests, it was evident that the laser surface texturing of the Al CC and the related slight increase in the surface oxygen content (see Section 3.1) did not have a detrimental effect on the electrochemical performances of the electrode, even at high current densities.

This effect was further evaluated by Cyclic Voltammetry (CV) measurements on both types of cells in the voltage range 2.8–4.3 V. Five cycles were performed at a scanning speed of 0.1 mV s^{-1}. As evidenced in Fig. 4a, the CV profiles of the textured and untextured electrodes are very similar. The redox peaks were associated with the phase transformations of NMC811 upon Li^+ intercalation/deintercalation. The peak current density was comparable, whereas the textured electrode

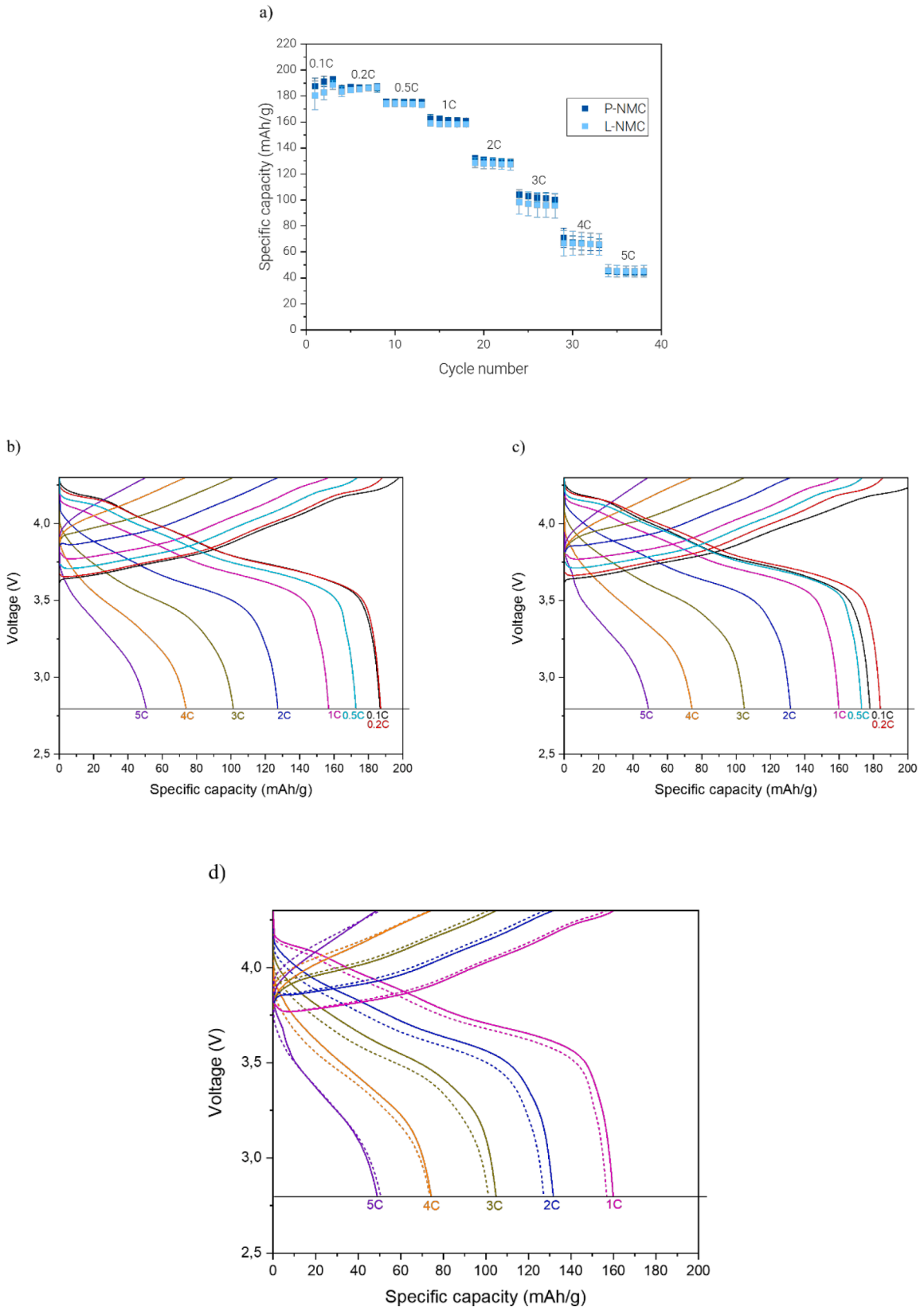

Fig. 3. a) Specific capacity vs cycle number plot of P-NMC and l-NMC half cells. Voltage vs Specific charge/discharge capacity for b) P-NMC and c) l-NMC half cells. d) Comparison of specific discharge capacity at increasing C-rates for P-NMC (dashed lines) and l-NMC (continuous lines).

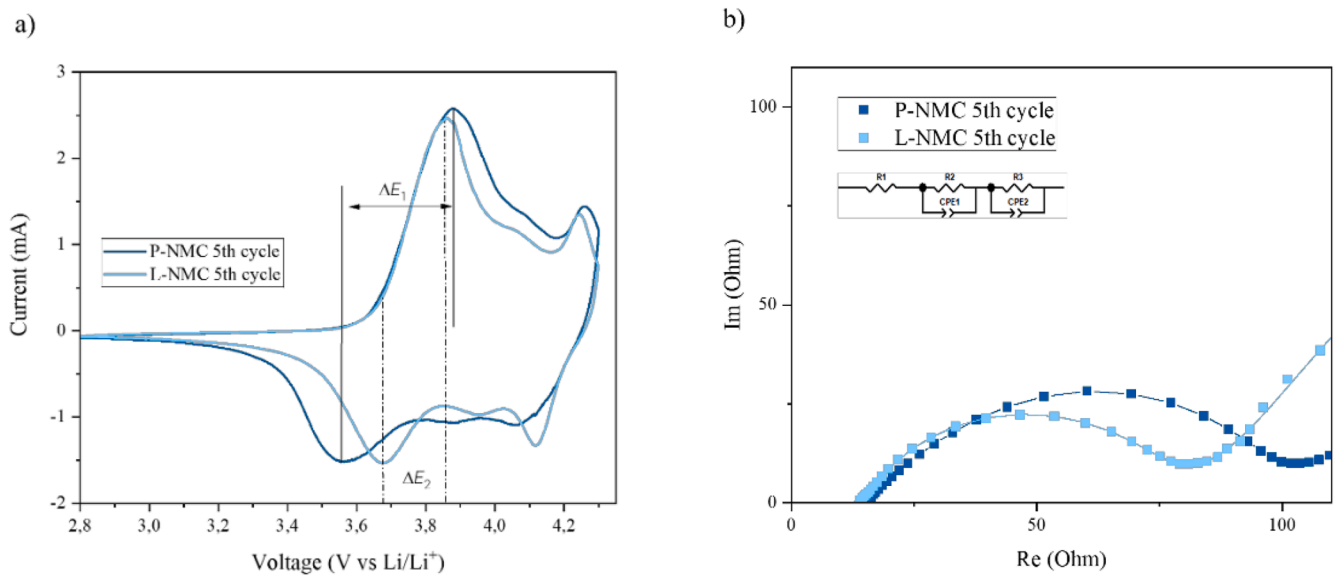

Fig. 4. a) CV curves of the 3rd scan for l-NMC and P-NMC electrodes. b) Nyquist plot of EIS data (dots) and related fits (lines) for l-NMC and P-NMC half-cell recorded after 5 cycles at C/10.

Table 3
Summary of the EIS fitting results of the two NMC electrodes.

Sample	R_1 (Ω)	R_2 (Ω)	R_3 (Ω)
P-NMC	15.47	40.03	49.63
L-NMC	14.42	38.19	31.33

displayed a lower peak separation (ΔE_2 = 193 mV) between the oxidation and reduction peaks compared to the untextured one (ΔE_1 =325 mV), highlighting its lower polarization. In addition, the l-NMC electrode displayed better resolved anodic and cathodic peaks, further highlighting the improved electrochemical reaction kinetics of the textured electrode.

The electrochemical properties of the electrodes were further analysed through Electrochemical Impedance Spectroscopy (EIS). To ensure the reliability of the measurements, uniform conditions were applied to the cells and the spectra were recorded after a complete charge/discharge cycle at C/10 for 5 cycles. The fifth cycle was selected for fitting using the ZView software. The fitting procedure was focused on retrieving the resistance values, and the Warburg element was not present in the selected equivalent circuit, as shown in Fig. 4b. The Nyquist plots of the two electrodes exhibited distinct characteristics: a high-frequency semi-circle and a low-frequency inclined profile. Herein, R_1 signifies the ohmic resistance, while R_2 and R_3 denote the Solid Electrolyte interphase (SEI) layer resistance and the charge-transfer resistance, respectively. Table 3 summarizes the fitting results. The R_1 and R_2 values were comparable, whereas the l-NMC electrode displayed the lower charge transfer resistance, further confirming the superior electrochemical properties of the textured electrode thanks to the increased surface area of the CC that ensured better electric charge transfer between the CC and active material.

To further evaluate the change in the cell resistance and the role of the laser surface texturing of the CC, the Intermitted Current Interruption (ICI) technique was employed. This method is an alternative to the Galvanostatic Intermitted Titration Technique and can render the same information about the Internal Resistance (IR) of the cell in a shorter

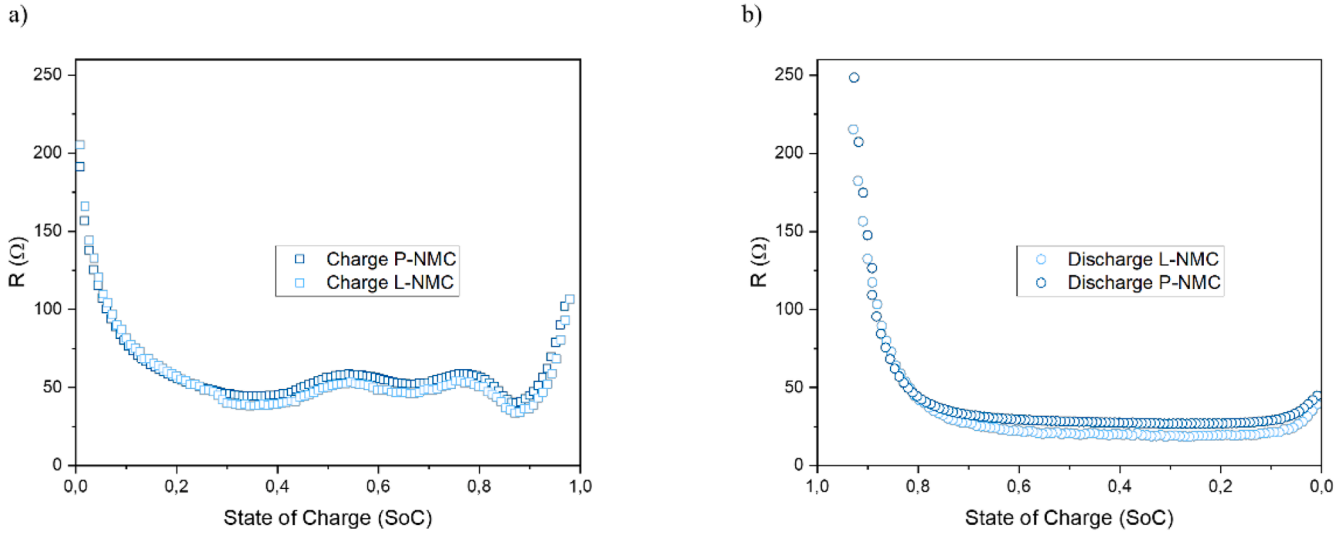

Fig. 5. Intermitted current titration techniques obtained values of the Internal Resistance of the cell for P-NMC and l-NMC electrodes both during charge and discharge half cycles.

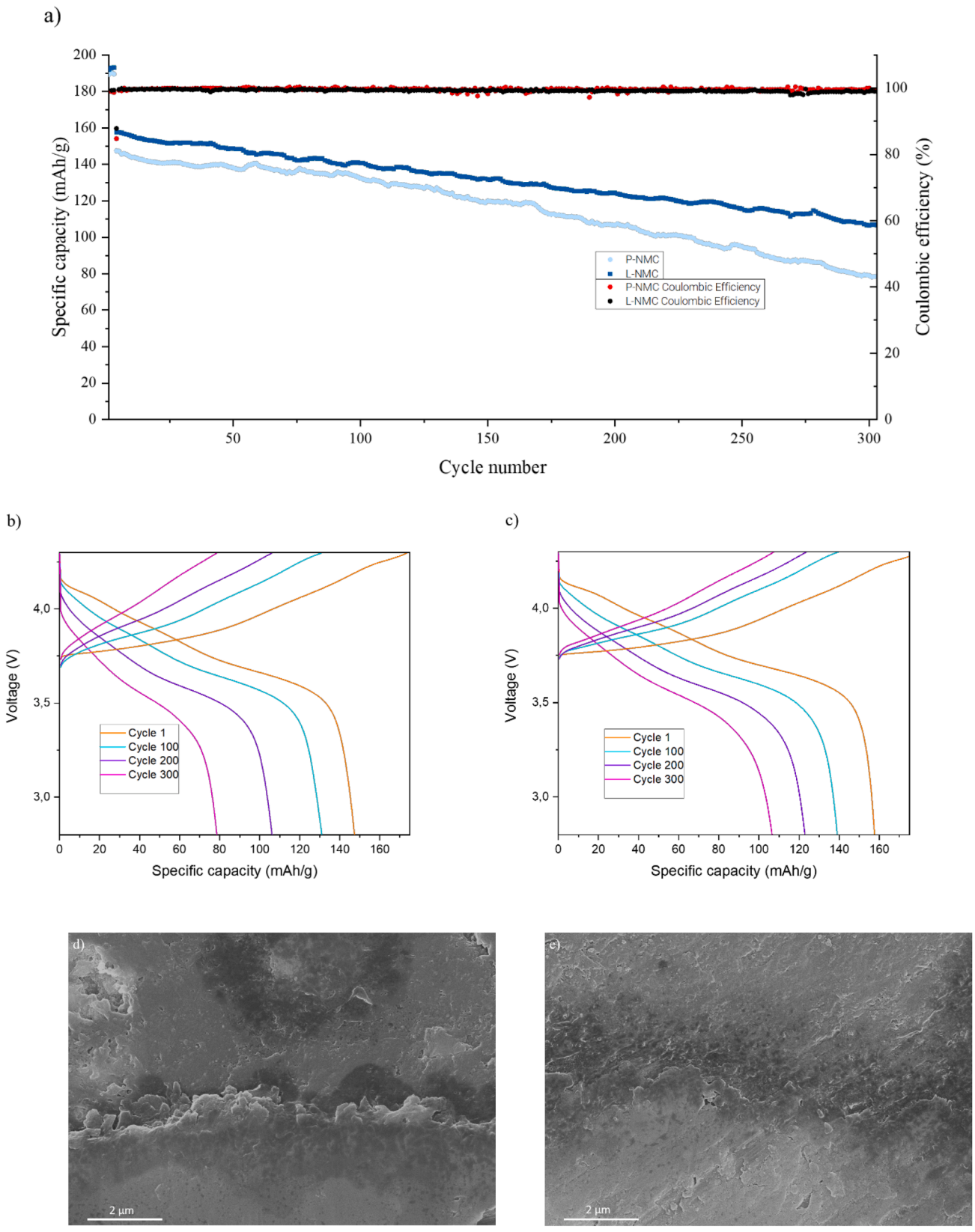

Fig. 6. a) Specific capacity vs cycle number plot of P-NMC and l-NMC half cells during long cycling experiments. Voltage vs Specific charge/discharge capacity for b) P-NMC and c) l-NMC half cells during long cycling experiments. SEM micrographs of the cycled a) P-NMC and b) l-NMC electrodes at a magnification of 30 kX.

Table 4
Values of specific capacity, coulombic efficiency and capacity retention for P-NMC and l-NMC electrodes.

Cycle number	P-NMC			L-NMC		
	Specific Capacity mAh g^{-1}	Coulombic Efficiency %	Capacity Retention %	Specific Capacity mAh g^{-1}	Coulombic Efficiency %	Capacity Retention %
5	144.52	99.29	98.06	155.99	99.62	98.9
10	142.85	99.71	96.92	154.14	99.70	97.76
50	137.16	99.85	93.07	147.58	99.48	93.6
100	131.22	99.78	89.04	139.02	99.18	88.2
200	106.40	99.65	72.19	122.89	99.19	77.9
300	78.55	99.54	53.30	106.61	99.02	67.6

time [33,34]. It is based on the application of a constant current at C/10 for 5 min followed by a short relaxation period of 5 s, and the evaluation of the voltage drop after switching off the current.

The results are shown in Fig. 5a-b, where it is evident that the IR of the cell is lower both during charge and discharge, at every State of Charge (SoC). More in detail, the IR of the P-NMC during charging oscillated between 45 Ω at 30% SoC and 59 Ω at 75% SoC, whereas the l-NMC displayed lower values between 40 Ω at 30% SoC and 54 Ω at 75% SoC. During discharge, the IR was shifted to lower values, but the overall better performances of the l-NMC electrode were confirmed (32 Ω and 19 Ω at 75% and 30% SOC respectively for the l-NMC, 36 Ω and 27 Ω at 75% and 30% SoC respectively for the P-NMC). This behaviour was consistent with previously reported results using NMC811 as active material [33]. In general, a battery's internal resistance comprises four components. Firstly, the ohmic resistance, also known as AC resistance, encompasses the electronic and ionic resistance across various parts like current collectors, terminals, electrodes, active material, electrolyte, and separator. Secondly, there is the resistance of the SEI formation, which begins during initial charge/discharge cycles and progressively increases during cycling and storage. The third element is the resistance associated with charge transfer during chemical reactions. Lastly, there is the resistance linked to the diffusion process, impacting mass transport within electrodes and electrolytes [35,36]. Higher internal resistance can limit the electrochemical performance of the battery.

The presented results are in agreement with the previous findings and further prove the superior electrochemical behaviour of the laser-textured current collector compared to the pristine one.

The l-NMC and the P-NMC cathodes were also subjected to long cycling experiments, at a constant C-rate of 1C for 300 cycles. As can be observed in Fig. 6a, the capacity retention after 100 cycles was 89% and 88.2% for P-NMC and l-NMC electrodes, respectively. Interestingly, higher differences were found increasing the number of cycles. The capacity retention for the P-NMC electrode was 72 % and 53.3%, whereas the l-NMC cell showed 78% and 67.6% after 200 and 300 cycles respectively. The coulombic efficiency was above 99 % for both the P-NMC and the l-NMC electrodes, even after 300 cycles. Values of specific capacity, coulombic efficiency, and capacity retention are reported in Table 4.

Charge and discharge curves and the related differential capacity curves after 100, 200 and 300 cycles are reported in Fig. 6b-c. As can be observed, the polarization of the cell increased during cycling due to materials degradation. Notably, the polarization was lower for the l-NMC compared to the P-NMC electrode, as already observed in the previous analyses. These results were probably related to the delamination of the active material particles, due to repeated volume contraction/expansion, and cracking upon deintercalation/deintercalation of Li^+ ions [37,38]. The increased adhesion of the active material coating donated by the laser surface texturing of the current collector was able to reduce this effect and improve the long-cycling stability of the electrode. To further investigate this aspect, after 300 cycles coin cells were opened and the electrodes were recovered to evaluate the interface between the CC and the active material. Moreover, the recovered electrodes were embedded in a resin and polished for cross-section analysis of the interface between the current collector and the coating by means of FESEM analysis. As evidenced in Fig. 6d-e, the P-NMC electrode exhibits a damaged interface, with small cracks that were responsible for the reduced electrochemical performances of the cell. On the other hand, the l-NMC electrode shows a good retained adhesion even after 300 cycles, with no evident signs of delamination. These results better clarify the role of the modified adhesive properties of the current collector and its relation to the previously reported electrochemical results.

4. Conclusions

A picosecond laser texturing method was proved to be a suitable technique to achieve the simultaneous increase of the adhesion, able to improve the cycling performances of the LIB, and the directional adhesion properties that can allow easy recyclability of the spent battery. By employing a parallel line scanning strategy with optimized scanning speed and line distance, asymmetric triangular features were generated on the CC surface. A large increase in surface area resulted in an augmented adhesion between the active coating and the current collector, with directional properties that are promising for the recyclability of the electrode. Despite this adhesion increase, the electrochemical performances were not affected at high current densities and there was no evidence of a substantial increase in the specific capacity delivered by the textured electrode. Nonetheless, the long cycling experiments showed promising results related to the diminished delamination of active material thanks to the modified adhesive properties of the Al surface. The l-NMC with a high mass loading of 8 mg cm^{-2} showed increased capacity retention up to 67.7% after 300 1C cycles, compared to 53.3% for the P-NMC electrode. The increased electrochemical performances were further proved using different electrochemical techniques that were able to give more insights into the underlying mechanisms of the interaction between the active material particles and the current collector surface. The outcomes of this study evidence the potentially pivotal role of laser-based techniques in the design of more efficient, sustainable and recyclable next-generation batteries.

CRediT authorship contribution statement

Paolo Tallone: Writing – original draft, Methodology, Investigation, Data curation. **Silvia Spriano:** Writing – review & editing, Supervision, Resources, Funding acquisition, Conceptualization. **Daniele Versaci:** Writing – review & editing, Validation, Supervision, Methodology, Investigation. **Sara Ferraris:** Writing – review & editing, Supervision, Resources, Funding acquisition. **Alice Tori:** Writing – review & editing, Project administration, Funding acquisition, Conceptualization. **Silvia Bodoardo:** Writing – review & editing, Supervision, Resources, Funding acquisition, Conceptualization.

Declaration of competing interest

The authors declare that they have no known competing financial

interests or personal relationships that could have appeared to influence the work reported in this paper.

Data availability

Data will be made available on request.

Acknowledgements

The authors would like to thank Anton Paar Italy S.r.l for their help in performing the mechanical test of the electrodes.

This publication is part of the project PNRR-NGEU which has received funding from the MUR – DM 352/2022.

Dr. Versaci D. acknowledges support from FSE REACT-EU - PON Ricerca e Innovazione 2014–2020 program (Ministerial Decree no. 1062/2021).

References

[1] J.T. Frith, M.J. Lacey, U. Ulissi, A non-academic perspective on the future of lithium-based batteries, Nat. Commun. 14 (1) (2023) 420, https://doi.org/10.1038/s41467-023-35933-2.

[2] Y. Yang, R. Wang, Z. Shen, Q. Yu, R. Xiong, W. Shen, Towards a safer lithium-ion batteries: a critical review on cause, characteristics, warning and disposal strategy for thermal runaway, Adv. Appl. Energy 11 (2023) 100146, https://doi.org/10.1016/j.adapen.2023.100146.

[3] J. Piątek, S. Afyon, T.M. Budnyak, S. Budnyk, M.H. Sipponen, A. Slabon, Sustainable Li-Ion Batteries: chemistry and Recycling, Adv. Energy Mater. 11 (43) (2021) 2003456, https://doi.org/10.1002/aenm.202003456.

[4] C. Ferrara, R. Ruffo, E. Quartarone, P. Mustarelli, Circular Economy and the Fate of Lithium Batteries: second Life and Recycling, Adv. Energy Sustain. Res. 2 (10) (2021) 2100047, https://doi.org/10.1002/aesr.202100047.

[5] G. Harper, et al., Recycling lithium-ion batteries from electric vehicles, Nature 575 (7781) (2019), https://doi.org/10.1038/s41586-019-1682-5. Art. 7781.

[6] G.D.J. Harper, et al., Roadmap for a sustainable circular economy in lithium-ion and future battery technologies, J. Phys. Energy 5 (2) (2023) 021501, https://doi.org/10.1088/2515-7655/acaa57.

[7] Z.J. Baum, R.E. Bird, X. Yu, J. Ma, Lithium-Ion Battery Recycling-Overview of Techniques and Trends, ACS Energy Lett. 7 (2) (2022) 712–719, https://doi.org/10.1021/acsenergylett.1c02602.

[8] Y. He, et al., A critical review of current technologies for the liberation of electrode materials from foils in the recycling process of spent lithium-ion batteries, Sci. Total Environ.s 766 (2021) 142382, https://doi.org/10.1016/j.scitotenv.2020.142382.

[9] R. Saneie, H. Abdollahi, S. Ghassa, D. Azizi, S. Chehreh Chelgani, Recovery of Copper and Aluminum from Spent Lithium-Ion Batteries by Froth Flotation: a Sustainable Approach, J. Sustain. Metall. 8 (1) (2022) 386–397, https://doi.org/10.1007/s40831-022-00493-0.

[10] C. Xing, et al., Aluminum Impurity from Current Collectors Reactivates Degraded NCM Cathode Materials toward Superior Electrochemical Performance, ACS. Nano 17 (3) (2023) 3194–3203, https://doi.org/10.1021/acsnano.3c00270.

[11] S. Natarajan, R.M. Bhattarai, M.S.P. Sudhakaran, Y.S. Mok, S.J. Kim, Recycling of spent graphite and copper current collector for lithium-ion and sodium-ion batteries, J. Power. Sources. 577 (2023) 233170, https://doi.org/10.1016/j.jpowsour.2023.233170.

[12] B.P. Thapaliya, et al., Enhancing Cycling Stability and Capacity Retention of NMC811 Cathodes by Reengineering Interfaces via Electrochemical Fluorination, Adv. Mater. Interfaces. 9 (18) (2022) 2200035, https://doi.org/10.1002/admi.202200035.

[13] H. Choi, S. Kim, H. Song, S. Suh, H.-J. Kim, K. Eom, Fabrication of a Porous Copper Current Collector Using a Facile Chemical Etching to Alleviate Degradation of a Silicon-Dominant Li-ion Battery Anode, Corr. Sci. Technol. 20 (5) (2021) 249–255, https://doi.org/10.14773/CST.2021.20.5.249.

[14] H. Jeong, J. Jang, C. Jo, A review on current collector coating methods for next-generation batteries, Chem. Eng. J. 446 (2022) 136860, https://doi.org/10.1016/j.cej.2022.136860.

[15] M. Onsrud, A.O. Tezel, S. Fotedar, A.M. Svensson, Novel carbon coating on aluminum current collectors for lithium-ion batteries, SN Appl. Sci. 4 (8) (2022) 225, https://doi.org/10.1007/s42452-022-05103-y.

[16] P. Zhu, D. Gastol, J. Marshall, R. Sommerville, V. Goodship, E. Kendrick, A review of current collectors for lithium-ion batteries, J. Power. Sources. 485 (2021) 229321, https://doi.org/10.1016/j.jpowsour.2020.229321.

[17] C. Lamiel, I. Hussain, X. Ma, K. Zhang, Properties, functions, and challenges: current collectors, Mater. Today Chem. 26 (2022) 101152, https://doi.org/10.1016/j.mtchem.2022.101152.

[18] M.G. Berhe, H.G. Oh, S.-K. Park, D. Lee, Laser cutting of silicon anode for lithium-ion batteries, J. Mater. Res. Technol. 16 (2022) 322–334, https://doi.org/10.1016/j.jmrt.2021.11.135.

[19] e T. Jansen, M. Kandula, S. Hartwig, L. Hoffmann, W. Haselrieder, K. Dilger, Influence of laser-generated cutting edges on the electrical performance of Large Lithium-Ion Pouch Cells, Batteries 5 (4) (2019) 73, https://doi.org/10.3390/batteries5040073.

[20] A. Sadeghian, N. Iqbal, A review on dissimilar laser welding of steel-copper, steel-aluminum, aluminum-copper, and steel-nickel for electric vehicle battery manufacturing, Opt. Laser Technol. 146 (2022) 107595, https://doi.org/10.1016/j.optlastec.2021.107595.

[21] W. Pfleging, A review of laser electrode processing for development and manufacturing of lithium-ion batteries, Nanophotonics. 7 (3) (2018), https://doi.org/10.1515/nanoph-2017-0044. Art. 3.

[22] M.-J. Kleefoot, et al., Enhancement of the wettability of graphite-based lithium-ion battery anodes by selective laser surface modification using low energy nanosecond pulses, Int. J. Adv. Manuf. Technol. 118 (5–6) (2022), https://doi.org/10.1007/s00170-021-08004-3. Art. 5–6.

[23] J.B. Habedank, et al., Rapid electrolyte wetting of lithium-ion batteries containing laser structured electrodes: in situ visualization by neutron radiography, Int. J. Adv. Manuf. Technol. 102 (9–12) (2019), https://doi.org/10.1007/s00170-019-03347-4.

[24] M. Gebrekiros Berhe, H.G. Oh, S.-K. Park, M. Mondal, D. Lee, Effect of laser-induced groove morphology on the wettability and performance of Lithium-ion batteries, Mater. Des. 231 (2023) 112020, https://doi.org/10.1016/j.matdes.2023.112020.

[25] L. Romoli, A.H.A. Lutey, G. Lazzini, Laser texturing of Li-ion battery electrode current collectors for improved active layer interface adhesion, CIRP Ann. 71 (1) (2022), https://doi.org/10.1016/j.cirp.2022.04.034. Art. 1.

[26] e E. Ravesio, A.H.A. Lutey, D. Versaci, L. Romoli, S. Bodoardo, Nanosecond pulsed laser texturing of Li-ion battery electrode current collectors: electrochemical characterisation of cathode half-cells, Sustain. Mater. Technol. 38 (2023) e00751, https://doi.org/10.1016/j.susmat.2023.e00751.

[27] Y. Wang, et al., Hierarchically micro/nanostructured current collectors induced by ultrafast femtosecond laser strategy for high-performance Lithium-ion Batteries, Energy Environ. Mater. 5 (3) (2022) 969–976, https://doi.org/10.1002/eem2.12223.

[28] Q. Li, et al., High-rate and excellent-cycle performance Li4Ti5O12 electrodes with 3D porous copper foils as current collectors fabricated using a femtosecond laser processing strategy, J. Energy Storage 62 (2023) 106915, https://doi.org/10.1016/j.est.2023.106915.

[29] N. Zhang, Y. Zheng, A. Trifonova, W. Pfleging, Laser structured Cu foil for high-performance lithium-ion battery anodes, J. Appl. Electrochem. 47 (7) (2017), https://doi.org/10.1007/s10800-017-1086-x.

[30] C. Jin, Z. Yang, J. Li, Y. Zheng, W. Pfleging, T. Tang, Bio-inspired interfaces for easy-to-recycle lithium-ion batteries, Extreme Mech. Lett. 34 (2020) 100594, https://doi.org/10.1016/j.eml.2019.100594.

[31] A. Gabryelczyk, S. Ivanov, A. Bund, G. Lota, Corrosion of aluminium current collector in lithium-ion batteries: a review, J. Energy Storage 43 (2021) 103226, https://doi.org/10.1016/j.est.2021.103226.

[32] P. Meister, et al., Anodic Behavior of the Aluminum Current Collector in Imide-Based Electrolytes: influence of Solvent, Operating Temperature, and Native Oxide-Layer Thickness, ChemSusChem. 10 (4) (2017) 804–814, https://doi.org/10.1002/cssc.201601636.

[33] Y.-C. Chien, H. Liu, A.S. Menon, W.R. Brant, D. Brandell, M.J. Lacey, Rapid determination of solid-state diffusion coefficients in Li-based batteries via intermittent current interruption method, Nat. Commun. 14 (1) (2023) 2289, https://doi.org/10.1038/s41467-023-37989-6.

[34] L. Yin, et al., Implementing intermittent current interruption into Li-ion cell modelling for improved battery diagnostics, Electrochim. Acta 427 (2022) 140888, https://doi.org/10.1016/j.electacta.2022.140888.

[35] H.-G. Schweiger, et al., Comparison of several methods for determining the internal resistance of Lithium Ion Cells, Sensors 10 (6) (2010) 5604–5625, https://doi.org/10.3390/s100605604.

[36] S. Barcellona, S. Colnago, G. Dotelli, S. Latorrata, L. Piegari, Aging effect on the variation of Li-ion battery resistance as function of temperature and state of charge, J. Energy Storage 50 (2022) 104658, https://doi.org/10.1016/j.est.2022.104658.

[37] e T. Li, X.-Z. Yuan, L. Zhang, D. Song, K. Shi, C. Bock, Degradation mechanisms and mitigation strategies of Nickel-Rich NMC-Based Lithium-Ion Batteries, Electrochem. Energ. Rev. 3 (1) (2020) 43–80, https://doi.org/10.1007/s41918-019-00053-3.

[38] F. Friedrich, et al., Editors' Choice—Capacity Fading Mechanisms of NCM-811 Cathodes in Lithium-Ion Batteries Studied by X-ray diffraction and other diagnostics, J. Electrochem. Soc. 166 (15) (2019) A3760–A3774, https://doi.org/10.1149/2.0821915jes.